ATLAS NOTE

July 26, 2015

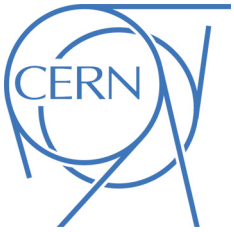

Prospect for a search for direct pair production of a chargino and a neutralino decaying via a W boson and the lightest Higgs boson in final states with one lepton, two b-jets and missing transverse momentum at the high luminosity LHC with the ATLAS Detector.

The ATLAS Collaboration

ATL-PHYS-PUB-2015-032
29 July 2015

Abstract

The current searches at the LHC have yielded sensitivity to electro-weakinos in the hundreds of GeV mass range. The reach at the high-luminosity phase of the LHC is expected to significantly extend beyond the current limits. This document presents example benchmark studies for chargino-neutralino production with the sparticles decaying via the W and lightest Higgs bosons (assumed SM like) with a parameterised simulation of the ATLAS detector at a centre-of-mass energy of 14 TeV. Results are shown for an integrated luminosity of 300 and 3000 fb^{-1}.

1 Introduction

Supersymmetry (SUSY) [1–9] proposes for every boson (fermion) of the Standard Model (SM) there exists a fermionic (bosonic) partner. The existence of SUSY particles with masses at the electroweak scale leads to contributions that can cancel quadratic divergences to the Higgs mass corrections. SUSY can also accommodate the unification of the gauge interactions and a radiative breaking of the electroweak symmetry. Under the conservation of R-parity, the lightest SUSY particle (LSP) is stable and is an excellent candidate to account for the dark matter in the universe. Furthermore, the minimal supersymmetric model (MSSM) requires a Higgs boson with mass below ~135 GeV which could be consistent with the recently observed Higgs-like resonance [10, 11]. The discovery (or exclusion) of weak-scale SUSY is one of the highest physics priorities for the current and future LHC, including the high luminosity upgrade, HL–LHC ($\sqrt{s}$ =14 TeV; 3000 fb^{-1}). The multi-TeV energy range probed with the LHC and the HL-LHC will not be accessible at any other current facility.

This note shows comparisons of the discovery and exclusion reach of ~300 fb^{-1} at the LHC and ~3000 fb^{-1} at the HL-LHC, both with $\sqrt{s}$=14 TeV pp collisions for chargino-neutralino production with the sparticles decaying via the W and lightest Higgs bosons (assumed SM like) assuming R-parity conserving SUSY.

1.1 The LHC and HL–LHC

In 2012, the LHC delivered 22.8 fb^{-1} of proton-proton collisions at a centre-of-mass-energy of 8 TeV. During the shutdown following the end of data-taking (LS1), the machine has been consolidated to be able to operate at a centre-of-mass-energy of 13 TeV, with the possibility of future 14 TeV collisions. In the present data taking period the LHC will collect ~100 fb^{-1}. A second long shutdown (LS2) will follow, during which the injection chain is foreseen to be modified to allow for instantaneous luminosities up to ~2×10^{34} cm^{-2}s^{-1}. The maximum average number of proton-proton collisions per bunch crossing is expected to be $\langle\mu\rangle \sim 60$ and the data collected up to the next long shutdown (LS3) will amount to ~300 fb^{-1}. During LS3, the accelerator is foreseen to be upgraded to the HL–LHC which will be able to achieve luminosities of ~7×10^{34} cm^{-2}s^{-1}. The HL–LHC is expected to deliver an average number of pile up events per bunch crossing of $\langle\mu\rangle \sim 200$ and the data collected will amount to ~3000 fb^{-1}. In the results reported here, however, the previous estimate of $\langle\mu\rangle \sim 140$ is used to parametrise the detector response. The increased pile up degrades the ability to reconstruct quantities like missing transverse momentum and therefore event numbers do not scale simply with integrated luminosity.

1.2 The ATLAS experiment

ATLAS [12] is a multipurpose particle physics detector with a forward-backward symmetric cylindrical geometry and nearly 4π coverage in solid angle[1]. The layout of the detector is dominated by four superconducting magnet systems, which comprise a thin solenoid surrounding inner tracking detectors (ID) with $|\eta| < 2.5$ and three large toroids supporting a large muon tracker (MS). The MS covers a range of $|\eta| < 2.7$ for precision measurements and $|\eta| < 2.4$ for triggering purposes. In the pseudorapidity region $|\eta| < 3.2$, high-granularity liquid-argon (LAr) electromagnetic (EM) sampling calorimeters surround the solenoid magnet. An iron-scintillator tile calorimeter provides hadronic coverage over $|\eta| < 1.7$. The endcap and forward regions, spanning $1.5 < |\eta| < 4.9$, are instrumented with LAr calorimeters for both EM and hadronic measurements. Upgrades to the detector and the triggering system are planned to adapt the experiment to the increasing instantaneous and integrated luminosity expected with the HL–LHC [13].

[1] ATLAS uses a right-handed coordinate system with its origin at the nominal interaction point in the centre of the detector and the z-axis along the beam pipe. Cylindrical coordinates (r, ϕ) are used in the transverse plane, ϕ being the azimuthal angle around the beam pipe. The pseudorapidity η is defined in terms of the polar angle θ by $\eta = -\ln\tan(\theta/2)$.

2 Searches for R-parity conserving SUSY

2.1 SUSY searches at the LHC

In the framework of generic R-parity conserving supersymmetric extensions of the SM, SUSY particles are produced in pairs and the LSP is stable. In a large fraction of the parameter space, the LSP is the lightest neutralino, where neutralinos ($\tilde{\chi}^0_j$, $j = 1, 2, 3, 4$) and charginos ($\tilde{\chi}^\pm_i$, $i = 1, 2$) are the mass eigenstates originating from the superposition of the SUSY partners of Higgs and electroweak gauge bosons (higgsinos and electroweak gauginos). The scalar partners of right-handed and left-handed fermions can mix to form two mass eigenstates, nearly degenerate in the case of first and second generation squarks and sleptons ($\tilde{q}$ and $\tilde{l}$), whilst possibly split in the case of bottom and top squarks (sbottom, $\tilde{b}$ and stop, $\tilde{t}$) and tau sleptons (stau, $\tilde{\tau}$). The lighter top squark mass eigenstate can be significantly lighter than the other squarks and the gluinos ($\tilde{g}$, the supersymmetric partners of the gluons).

The ATLAS Collaboration is currently carrying out a broad programme of searches [14] including searches for light-flavour squarks and gluinos, weakly produced sparticles, and third generation squarks. Results from the searches mentioned above have excluded first and second generation squark and gluino masses below about 850 GeV and 1330 GeV, respectively, under the assumption of a simplified model and a very light LSP. Less stringent limits are placed on third generation squarks, charginos, neutralinos and sleptons. In particular, for the search described in this document, the current observed 95% CL limits exclude $\tilde{\chi}^0_2$,$\tilde{\chi}^\pm_1$ masses up to 250 GeV under the assumption of a massless LSP. The mass constraints strongly depend on the assumed SUSY mass spectrum.

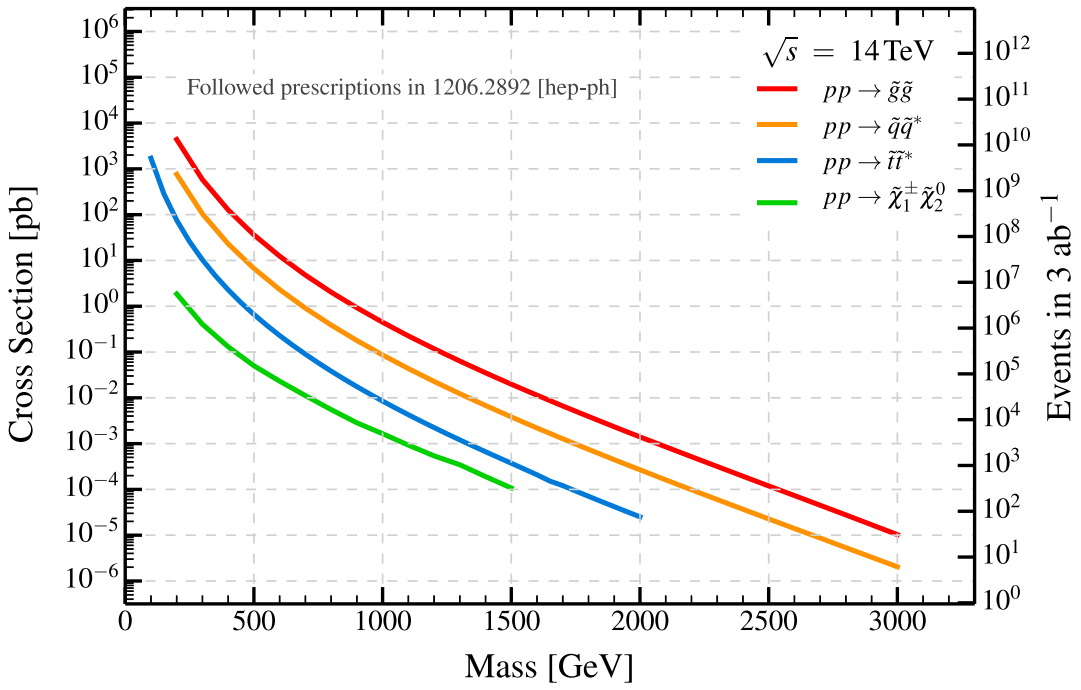

Figure 1: Next-to-leading order cross-sections for the production of supersymmetric particles at the LHC as a function of the average mass of the pair-produced supersymmetric particles. The $\tilde{\chi}^\pm_1$ and $\tilde{\chi}^0_2$ are assumed to be wino-like. Cross-sections for bottom squark pair production are equal to those of top squark pair production . The squark cross sections are shown for decoupled gluinos and the gluino cross section is shown for decoupled squarks.

2.2 SUSY searches at the HL–LHC

Previous studies of the discovery and exclusion reach of the HL-LHC have been carried out for squark and gluino production, for the production of top and bottom squarks and for the production of charginos and neutralinos [15, 16]. This note updates the searches for direct production of a neutralino and a chargino which decay to a W and a Higgs boson respectively and the LSP, with parameterisations of the upgraded ATLAS detector configurations and re-optimised selections, under the assumptions of:

- 300 fb^{-1} at $\sqrt{s}$= 14 TeV and $\langle\mu\rangle \sim 60$ (LHC)
- 3000 fb^{-1} at $\sqrt{s}$= 14 TeV and $\langle\mu\rangle \sim 140$ (HL–LHC).

For these analyses, Monte Carlo (MC) generator level information is used for both the background and the signal processes. The detector response is a parameterisation of the upgraded ATLAS detector performance based on Monte Carlo samples using full simulation of the upgraded detector in high pile-up conditions, as described in Refs. [17, 18]. The parameterisations describe the resolution and the reconstruction efficiencies of electrons, muons, jets, b-jets and missing transverse momentum. The mis-identification of c-jets and light flavour jets as b-jets is accounted for in the parameterisations. The parameterised response functions account for the effect of the number of interactions per bunch crossing ranging between 60 and 140 with 25ns bunch spacing. The effect of the trigger is not taken into account in these analyses, but planned upgrades to the detector, in particular an improved barrel muon coverage, are expected to allow lepton triggers that would have high efficiency for the studied scenarios with respect to the analysis selections.

2.3 Monte Carlo Generation

Several Monte Carlo generators are used to model the dominant SM processes and new physics signals relevant for the analyses. Sherpa-1.4.1 [19] is used to simulate the top pair, $W^{(*)}$+jets, and $Z^{(*)}$+jets processes. Sherpa-2.1 is used to simulate the vector boson pair production processes. All the Sherpa processes were generated with massive b, c quarks. The processes Zh and Wh are generated with Pythia-8.165 [20] and normalised to MCFM predictions [21]. The generator MadGraph-5.0 [22] is used for the production of $t\bar{t} + V$ ($V = W, Z$) events. Single top production is generated with AcerMC [23] for the t-channel, and Powheg [24]+Pythia for the Wt and s-channel processes. The top quark pair-production contribution is normalised to approximate next-to-next-to-leading-order calculations (NNLO) [25]. The expected W+jets, Z+jets and diboson yields are normalised to the Sherpa predictions. The expected $tt + V$ yields are normalised to NLO. The CTEQ6L1 [26] parton distribution functions (PDFs) are used with MadGraph and the CT10 [27] PDFs with Sherpa.

The signal MC samples are produced with Herwig++2.5.2 [28]. The yields are normalised to the NLO cross-section calculated with Prospino2 [29]. The most relevant MC samples have equivalent luminosity (at 14 TeV) of at least 1000 fb^{-1}.

3 Search for the direct production of charginos and neutralinos

Based on naturalness arguments, the $\tilde{\chi}_1^\pm$, $\tilde{\chi}_2^0$, and $\tilde{\chi}_1^0$ are expected to have masses in the hundreds of GeV range [30, 31] and are potentially within reach of the LHC. As seen in Fig. 1, the cross-section of $\tilde{\chi}_1^\pm\tilde{\chi}_2^0$ associated production ranges from 1000 to 10 fb for masses between 200 and 600 GeV and can dominate the SUSY production in scenarios with heavy squarks and gluinos.

One simplified model of direct production of $\tilde{\chi}_1^\pm$ and $\tilde{\chi}_2^0$ is studied in this note: all sleptons and sneutrinos are assumed to be heavy, both $\tilde{\chi}_1^\pm$ and $\tilde{\chi}_2^0$ are assumed to be wino-like with equal masses,

and the $\tilde{\chi}_1^0$ to be bino-like. The $\tilde{\chi}_1^\pm$ and $\tilde{\chi}_2^0$ decay via W and lightest Higgs boson, respectively, with a branching fraction of 100%. The Higgs boson considered is SM-like, with a mass of 125 GeV and is assumed to decay with SM branching ratios. Only the case where the Higgs decays to two b-quarks is studied for this scenario. The final state considered contains one lepton, two b-jets and missing transverse momentum as shown in Fig. 2.

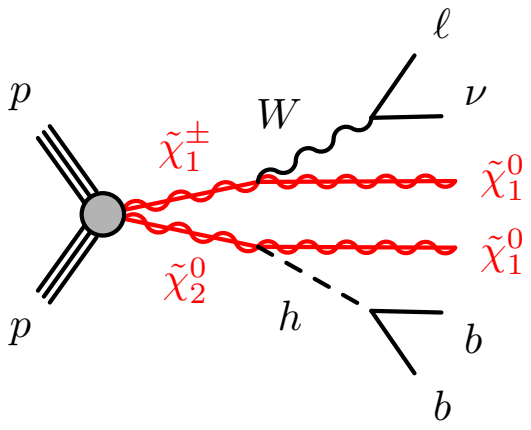

Figure 2: The diagram for the $\tilde{\chi}_2^0\tilde{\chi}_1^\pm$ simplified model studied in this note. The $\tilde{\chi}_1^\pm$ is assumed to decay as $\tilde{\chi}_1^\pm \to W^{\pm(*)}\tilde{\chi}_1^0$ and the $\tilde{\chi}_2^0$ as $\tilde{\chi}_2^0 \to h^{(*)}\tilde{\chi}_1^0$ with 100% branching ratio. One final state is studied for the Wh-mediated scenario: $1\ell 2b$.

The expected background is dominated by $t\bar{t}$, single top and associated production of $t\bar{t}$ and a vector boson ($t\bar{t}+V$).

3.1 Signal Region Selection

The event preselection is based on that of the 8 TeV analysis documented in [32]. Candidate leptons are selected with p_{T} larger than 25 GeV and $|\eta| < 2.47$ (2.4) for electrons (muons). Candidate jets are reconstructed with the anti-k_t algorithm with a radius parameter of 0.4, with $p_{\mathrm{T}} > 50$ GeV and $|\eta| < 2.5$. Jets are required to be separated from candidate electrons by $\Delta R(e, jet) > 0.2$, where $\Delta R \equiv \sqrt{(\Delta\phi)^2 + (\Delta\eta)^2}$. Jets are tagged as originating from b-decays (b-tagged) using a parameterisation (function of the jet p_{T} and η) modelling the performances of the IP3D+SV1 b-tagging algorithm. The chosen working point identifies b-jet with an average efficiency of 70%, a c-quark jets misidentification probability of about 20% and a light-flavour jet misidentification probability of about 1%. The truth $E_{\mathrm{T}}^{\mathrm{miss}}$ is computed as the vectorial sum of the momenta of neutral weakly-interacting particles (neutrinos and neutralinos). It is then smeared to simulate detector response, with a function parameterised in the average number of interactions per bunch crossing μ and the scalar sum of energy in the calorimeter $\sum E_{\mathrm{T}}$.

Events are selected with exactly one high energetic and isolated lepton. The isolation criteria is defined by asking that $\Delta R(\ell, jet) > 0.4$. Events with additional leptons are vetoed. The event must contain at least two b-tagged jets, that, in addition, must be the leading jets in the event.

The invariant mass computed from the b-jets momenta is required to be in the range $105 < m_{bb} < 135$ GeV, to reject non-resonant SM backgrounds. This cut has an average efficiency on signal events of 65% in the $\langle\mu\rangle = 60$ scenario. This efficiency degrades by up to 5% passing to the $\langle\mu\rangle = 120$ scenario, however modifying the mass selection was found to have negligible effects on the final SR sensitivity and hence kept the same. Furthermore, the events are required to contain fewer than four jets, to reduce the contamination coming from semi-leptonic and fully hadronic $t\bar{t}$ events. Since the final state contains two

$\tilde{\chi}_1^0$ and one neutrino from the W decay, the resulting $E_{\mathrm{T}}^{\mathrm{miss}}$ spectrum in general extends to higher values than the major SM backgrounds: a selection cut $E_{\mathrm{T}}^{\mathrm{miss}} > 200$ GeV has been applied.

Starting from this common pre-selection, two alternative signal selection strategies have been investigated.

The first strategy closely follows that of the 8 TeV analysis. The main variables used to discriminate the chargino-neutralino pair from background are: the event $E_{\mathrm{T}}^{\mathrm{miss}}$, the transverse mass m_{T} (calculated using the lepton and $E_{\mathrm{T}}^{\mathrm{miss}}$) and the boost-corrected contransverse mass, m_{CT} [33]. For parent particles produced with small transverse boosts, m_{CT} is bounded from above by an analytical combination of particle masses. This bound is saturated when the two visible objects are co-linear and is in general given by:

$$m_{\mathrm{CT}}^{\mathrm{max}} = \frac{m_{parent}^2 - m_{daughter}^2}{m_{parent}}. \tag{1}$$

For $t\bar{t}$ events this kinematic bound is at 135 GeV. For events with highly-boosted $b\bar{b}$ resonances such as the production of chargino-neutralino pairs, m_{CT} extends to high values of and thus preferentially pass lower bounds on m_{CT}. Figure 3 shows the m_{CT} distribution for chargino-neutralino signal events for $\langle\mu\rangle = 60$ and $\langle\mu\rangle = 140$. Due to the endpoint for the $t\bar{t}$ process, the m_{CT} cut is found to be very effective in suppressing this background. The remaining $t\bar{t}$ events beyond the expected endpoint are due to the wrong selection of a mis-tagged c-quark jet from W decays as one of the selected b-jets. Figures 4 and 5 show respectively the distributions of m_{T} and $E_{\mathrm{T}}^{\mathrm{miss}}$; the variable m_{T} is useful for discriminating against SM backgrounds, particularly those involving leptonic decays of the W boson with no other source of $E_{\mathrm{T}}^{\mathrm{miss}}$. Background events can exceed the expected m_{T} endpoint because of the $E_{\mathrm{T}}^{\mathrm{miss}}$ resolution.

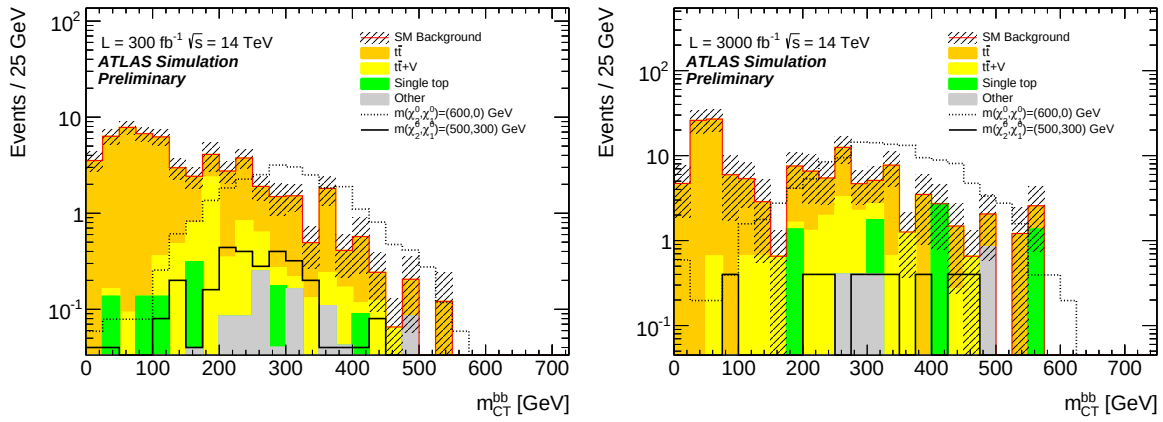

(a) 300 fb^{-1} $< \mu >= 60$ scenario

(b) 3000 fb^{-1} $< \mu >= 140$ scenario

Figure 3: Distributions of the b-jet pair m_{CT} after all the SRA (left) and SRC (right) selections but for the cut on m_{CT} itself. The contributions from all SM backgrounds are shown, with the bands representing the total uncertainty. The distributions of the signal expected for two different models are also shown: the solid line corresponds to a signal with a 500 GeV $\tilde{\chi}_2^0$,$\tilde{\chi}_1^{\pm}$ and a 300 GeV $\tilde{\chi}_1^0$ neutralino, while the dashed line corresponds to a signal with 600 GeV $\tilde{\chi}_2^0$,$\tilde{\chi}_1^{\pm}$ and a massless $\tilde{\chi}_1^0$.

The thresholds on m_{CT}, m_{T} and $E_{\mathrm{T}}^{\mathrm{miss}}$ are optimised for high discovery Z_N [34], defined to be

$$Z_n = \sqrt{2} erf^{-1}(1 - 2p) \tag{2}$$

where p indicates the p-value and erf^{-1} is the inverse error function. A systematic uncertainty of 30% on the estimated sum of all backgrounds is assumed, which is consistent with the uncertainties found

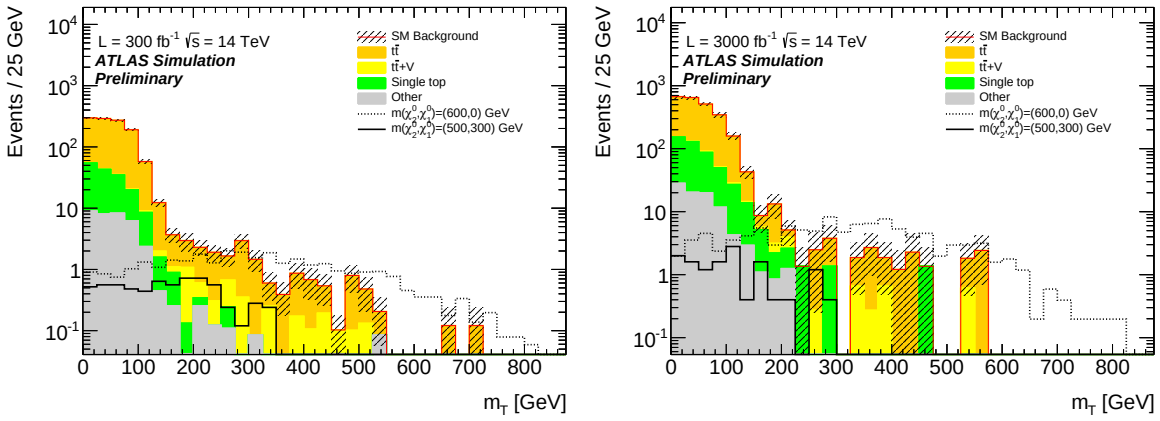

(a) 300 fb^{-1} < μ >= 60 scenario

(b) 3000 fb^{-1} < μ >= 140 scenario

Figure 4: Distributions of the event m_T after all the SRA (left) and SRC (right) selections but for the cut on m_T itself.The contributions from all SM backgrounds are shown, with the bands representing the total uncertainty. The distributions of the signal expected for two different models are also shown: the solid line corresponds to a signal with a 500 GeV $\tilde{\chi}_2^0$,$\tilde{\chi}_1^\pm$ and a 300 GeV $\tilde{\chi}_1^0$ neutralino, while the dashed line corresponds to a signal with 600 GeV $\tilde{\chi}_2^0$,$\tilde{\chi}_1^\pm$ and a massless $\tilde{\chi}_1^0$.

in published searches. Four signal regions are defined: two regions, "A" and "B", optimised for the 300 fb^{-1} scenario and two tighter regions, "C" and "D", optimised for the 3000 fb^{-1} scenario. These are summarised in Table 1.

Selection	SRA	SRB	SRC	SRD
# of leptons (e, μ)	1			
# b-tagged jets	2			
m_{bb} [GeV]	$105 < m_{bb} < 135$			
# jets	2 or 3			
m_{CT} [GeV]	> 200	> 200	> 300	> 300
m_T [GeV]	> 200	> 250	> 200	> 250
E_T^{miss} [GeV]	> 300	> 350	> 400	> 450
$\langle\mu\rangle$ = 60, 300 fb^{-1} scenario	yes	yes	–	–
$\langle\mu\rangle$ = 140, 3000 fb^{-1} scenario	–	–	yes	yes

Table 1: Summary of selection requirements for the Wh-mediated signal regions.

The second strategy uses boosted decision trees (BDT) to separate signal events from SM backgrounds, and is considered only in the HL-LHC scenario. The following variables are given as input to the BDT, after applying the common event pre-selection: m_{CT}, m_T, E_T^{miss}, ΔR(leading b-jet, sub-leading b-jet), the leading b-jet p_T and $\Delta\phi$(leading b-jet,E_T^{miss}).

Figure 6 shows the distributions of the additional variables not used in the cut and count approach.

Three BDTs were used: one targeting low values of the $\tilde{\chi}_2^0$,$\tilde{\chi}_1^\pm$ mass ($m(\tilde{\chi}_2^0,\tilde{\chi}_1^\pm)$ = 300 GeV, $m(\tilde{\chi}_1^0)$ = 0 GeV), one targeting intermediate masses ($m(\tilde{\chi}_2^0,\tilde{\chi}_1^\pm)$ = 800 GeV, $m(\tilde{\chi}_1^0)$ = 400 GeV) and the last one targeting heavier masses ($m(\tilde{\chi}_2^0,\tilde{\chi}_1^\pm)$ = 1300 GeV, $m(\tilde{\chi}_1^0)$ = 0 GeV). Each BDT was trained using a

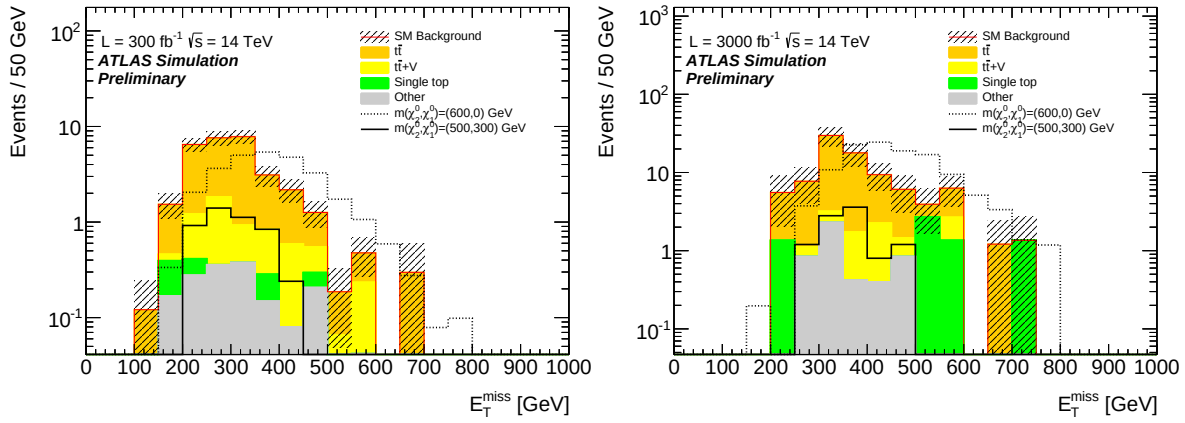

(a) 300 fb^{-1} < μ >= 60 scenario

(b) 3000 fb^{-1} < μ >= 140 scenario

Figure 5: Distributions of the event $E_{\mathrm{T}}^{\mathrm{miss}}$ after all the SRA (left) and SRC (right) selections but for the cut on $E_{\mathrm{T}}^{\mathrm{miss}}$ itself. The contributions from all SM backgrounds are shown, with the bands representing the total uncertainty. The distributions of the signal expected for two different models are also shown: the solid line corresponds to a signal with a 500 GeV $\tilde{\chi}_2^0$,$\tilde{\chi}_1^{\pm}$ and a 300 GeV $\tilde{\chi}_1^0$ neutralino, while the dashed line corresponds to a signal with 600 GeV $\tilde{\chi}_2^0$,$\tilde{\chi}_1^{\pm}$ and a massless $\tilde{\chi}_1^0$.

signal model and the requirement on the BDT output was optimised maximising Z_N for each of the BDTs. Three SRs were defined, which are shown in Table 2, after applying a common selection cut on $E_{\mathrm{T}}^{\mathrm{miss}} > 200$ GeV and $105 < m_{bb} < 135$ GeV. An example of the BDT output is shown in Fig. 7.

SR	Training Sample [GeV] $(m(\tilde{\chi}_2^0,\tilde{\chi}_1^{\pm}), m(\tilde{\chi}_1^0))$	BDT range
M1	(300,0)	> 0.22
M2	(800,400)	> 0.35
M3	(1300,0)	> 0.28

Table 2: Signal regions for the MVA analysis. The first column gives the name of each SR. The second column gives the signal sample used to train the BDT. The third column lists the selection requirements applied on the BDT output. All signal regions include a preselection cut on $E_{\mathrm{T}}^{\mathrm{miss}} > 200$ GeV and $105 < m_{bb} < 135$ GeV.

3.2 Expected Sensitivity

For the analyses discussed in this document, limits are set using Z_N: the value of Z_N is required to be larger than 5 for discovery and larger than 1.64 for 95% confidence level (CL) exclusion [2].

The same systematic uncertainty of 30% used for SR optimisation is assumed. Theoretical uncertainties on the SUSY signal are not found to have large effects on the limits for chargino-neutralino production. Experimental uncertainties on the SUSY yields have not been considered.

[2] A one sided confidence interval is used. Comparing the used prescription with a dedicated 95%CL exclusion test yields very similar results.

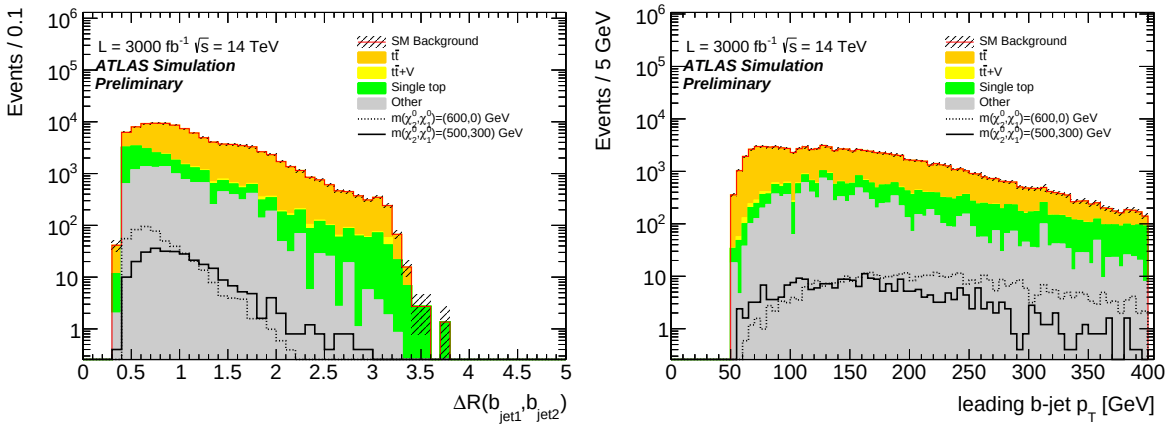

(a) ΔR(leading b-jet, sub-leading b-jet)

(b) Leading b-jet p_{T}

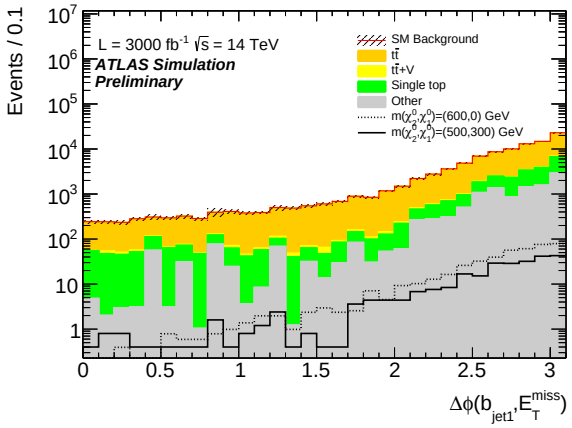

(c) $\Delta\phi$(leading b-jet,$E_{\mathrm{T}}^{\mathrm{miss}}$)

Figure 6: Distributions of the additional input variables to the BDT after the common preselection. The contributions from all SM backgrounds are shown, with the bands representing the total uncertainty. The distributions of the signal expected for two different models are also shown: the solid line corresponds to a signal with a 500 GeV $\tilde{\chi}_2^0$,$\tilde{\chi}_1^{\pm}$ and a 300 GeV $\tilde{\chi}_1^0$ neutralino, while the dashed line corresponds to a signal with 600 GeV $\tilde{\chi}_2^0$,$\tilde{\chi}_1^{\pm}$ and a massless $\tilde{\chi}_1^0$.

Tables 3 and 4 show the expected number of events for the SM background and three SUSY scenarios respectively for the 300 fb^{-1} and the 3000 fb^{-1} signal regions of the cut and count approach. The SM background is dominated by $t\bar{t}$ production in all signal regions, followed by contributions from single top and $t\bar{t}+V$ production. SM backgrounds with one mis-identified or non-prompt lepton are completely suppressed in this study by the tight signal regions requirements.

The 95% CL exclusion and 5σ discovery contours that would be expected for the Wh-mediated simplified models using the cut and count technique can be seen in Figure 8. For each signal model, the SR with the best expected discovery significance has been chosen. In the case of the Wh-mediated simplified models and the luminosity scenario of 300 fb^{-1}, the 95% CL exclusion contour reaches 920 GeV in $\tilde{\chi}_1^{\pm}$,$\tilde{\chi}_2^0$ mass, while for the high luminosity scenario with 3000 fb^{-1}, the contour extends up to 1120 GeV in $\tilde{\chi}_1^{\pm}$,$\tilde{\chi}_2^0$ mass. The discovery sensitivity reaches 790 GeV in $\tilde{\chi}_1^{\pm}$,$\tilde{\chi}_2^0$ mass for the high luminosity scenario with 3000 fb^{-1}, while no discovery reach is expected in the 300 fb^{-1} case. For this scenario, a three sigma "observation" line is shown instead, covering $\tilde{\chi}_1^{\pm}$,$\tilde{\chi}_2^0$ masses between 340 and 670 GeV for a

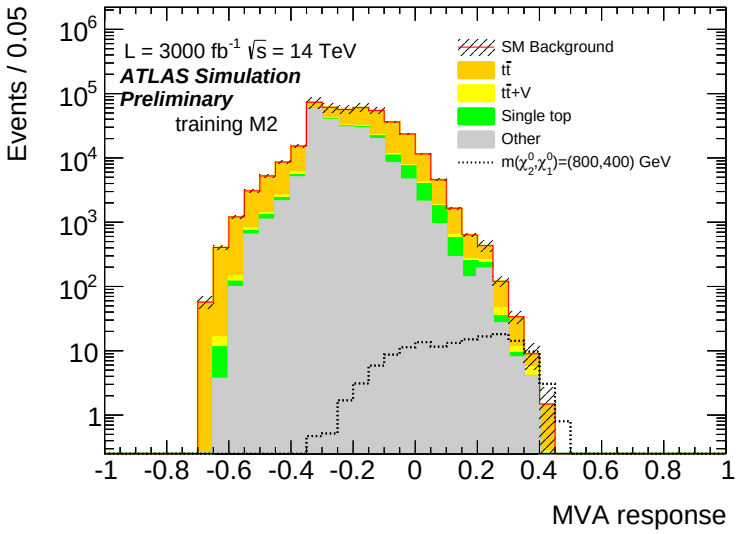

Figure 7: Distribution of the output BDT for the M2 training after the common preselection. The contributions from all SM backgrounds are shown, with the bands representing the statistical uncertainty. The expected distribution of the signal for the model used for the MVA training, corresponding to a signal with 800 GeV $\tilde{\chi}_2^0$,$\tilde{\chi}_1^\pm$ and a 400 GeV $\tilde{\chi}_1^0$ is shown by the dashed line.

	SRA	SRB
Expected events	14.9 ± 1.6	5.9 ± 0.9
$t\bar{t}$ events	12.1 ± 1.6	4.4 ± 0.9
single top events	0.23 ± 0.16	0.14 ± 0.14
$t\bar{t}+V$ events	2.1 ± 0.4	1.33 ± 0.29
Other SM events	0.42 ± 0.19	–
$m(\tilde{\chi}_2^0,\tilde{\chi}_1^\pm)$ = 600 GeV, $m(\tilde{\chi}_1^0)$ = 0 GeV events	23.2 ± 0.9	15.8 ± 0.6
$m(\tilde{\chi}_2^0,\tilde{\chi}_1^\pm)$ = 500 GeV, $m(\tilde{\chi}_1^0)$ = 300 GeV events	2.33 ± 0.32	0.46 ± 0.14
$m(\tilde{\chi}_2^0,\tilde{\chi}_1^\pm)$ = 1000 GeV, $m(\tilde{\chi}_1^0)$ = 0 GeV events	3.26 ± 0.13	2.79 ± 0.11

Table 3: Expected cut and count signal region yields, for an integrated luminosity of 300 fb^{-1}. The errors shown are the statistical uncertainties. The contribution listed as "Other SM" includes W+jets, $Z/\gamma*$+jets, diboson, Higgs boson production.

massless $\tilde{\chi}_1^0$.

Table 5 shows the expected number of events for the SM background and three SUSY scenarios respectively for the MVA signal regions with 3000 fb^{-1}. The SM background is dominated by $t\bar{t}$ production in all signal regions, followed by contributions from single top, W+jets and $t\bar{t}+V$ production. As in the cut-and-count approach, SM backgrounds with one mis-identified or non-prompt lepton are completely suppressed in this study by the tight signal regions requirements, that implicitly select events with large $E_{\mathrm{T}}^{\mathrm{miss}}$.

The 95% CL exclusion and 5σ discovery contours that would be expected for the Wh-mediated simplified models using the MVA technique can be seen in Fig. 9. The MVA improves the cut-and-count 95% CL exclusion sensitivity in the 3000 fb^{-1}scenario by 140 GeV, reaching 1310 GeV in $\tilde{\chi}_1^\pm$,$\tilde{\chi}_2^0$

	SRC	SRD
Expected events	30 ± 6	15 ± 4
$t\bar{t}$ events	18 ± 5	11 ± 4
single top events	5.4 ± 2.7	2.7 ± 1.9
$t\bar{t}$ + V events	3.8 ± 1.5	1.9 ± 1.1
Other SM events	2.8 ± 2.2	–
$m(\tilde{\chi}_2^0,\tilde{\chi}_1^\pm)$ = 600 GeV, $m(\tilde{\chi}_1^0)$ = 0 GeV events	83.7 ± 3.3	51 ± 4
$m(\tilde{\chi}_2^0,\tilde{\chi}_1^\pm)$ = 500 GeV, $m(\tilde{\chi}_1^0)$ = 300 GeV events	2.1 ± 0.9	0.8 ± 0.6
$m(\tilde{\chi}_2^0,\tilde{\chi}_1^\pm)$ = 1000 GeV, $m(\tilde{\chi}_1^0)$ = 0 GeV events	20.0 ± 0.8	16.8 ± 0.7

Table 4: Expected cut and count signal region yields, for an integrated luminosity of 3000 fb^{-1}. The errors shown are the statistical uncertainties. Entries marked – indicate a negligible background contribution. The contribution listed as "Other SM" includes W+jets, $Z/\gamma*$+jets, diboson and Higgs boson production.

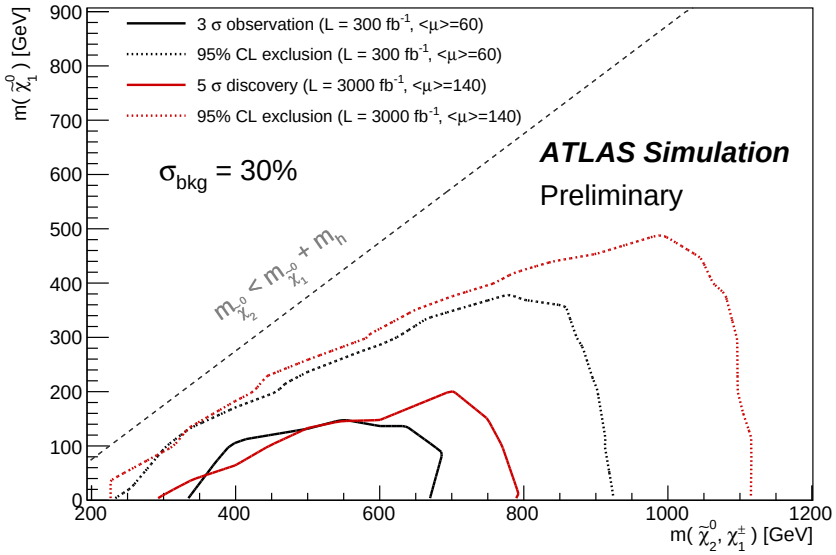

Figure 8: Expected sensitivity contours for the 300 fb^{-1} and 3000 fb^{-1} luminosity scenarios in the m($\tilde{\chi}_1^0$) vs m($\tilde{\chi}_1^\pm$,$\tilde{\chi}_2^0$) plane for the Wh-mediated simplified model, using the cut and count approach. The 5σ discovery contour is shown only for the the 3000 fb^{-1} scenario, while a 3 σ observation contour is shown for the 300 fb^{-1} scenario, where no 5 σ reach is expected. The degradation of the discovery sensitivity observed for values of m($\tilde{\chi}_1^\pm$,$\tilde{\chi}_2^0$) close to 400 GeV is due to the increased pile up effects and could be recovered with a dedicated optimisation in case of an early observation. 95% CL exclusion contours are shown for both scenarios.

mass for a massless $\tilde{\chi}_1^0$. The discovery contour is also extended, reaching 950 GeV in $\tilde{\chi}_1^\pm$,$\tilde{\chi}_2^0$ mass for a massless $\tilde{\chi}_1^0$.

	M1	M2	M3
Expected events	73 ± 12	10 ± 4	10 ± 4
$t\bar{t}$ events	58 ± 11	4.7 ± 2.9	8 ± 4
single top events	4.1 ± 2.4	–	–
W+jets events	4.1 ± 2.9	4.0 ± 2.8	–
$t\bar{t}+V$ events	4.5 ± 1.5	1.8 ± 1.0	1.5 ± 0.9
Other SM events	2.5 ± 1.5	–	–
$m(\tilde{\chi}_2^0,\tilde{\chi}_1^\pm)$ = 600 GeV, $m(\tilde{\chi}_1^0)$ = 0 GeV events	77 ± 5	69 ± 5	59 ± 4
$m(\tilde{\chi}_2^0,\tilde{\chi}_1^\pm)$ = 500 GeV, $m(\tilde{\chi}_1^0)$ = 300 GeV events	9.1 ± 2.0	1.2 ± 0.7	1.2 ± 0.7
$m(\tilde{\chi}_2^0,\tilde{\chi}_1^\pm)$ = 1000 GeV, $m(\tilde{\chi}_1^0)$ = 0 GeV events	11.2 ± 0.4	15.7 ± 0.6	18.9 ± 0.7

Table 5: Expected MVA signal region yields, for an integrated luminosity of 3000 fb^{-1}. The errors shown are the statistical uncertainties. Entries marked – indicate a negligible background contribution. The contribution listed as "Other SM" includes $Z/\gamma*$+jets, diboson and Higgs boson production.

4 Conclusions

The sensitivity to heavy SUSY particles will be increased significantly when the centre-of-mass-energy of the LHC reaches a value close to the design of $\sqrt{s}$ = 14 TeV. Feasibility studies on benchmark SUSY scenarios for chargino neutralino production are carried out with 14 TeV MC samples and by applying detector response corrections to generator level particles. An increase of integrated luminosity from 300 fb^{-1} to 3000 fb^{-1} extends significantly the discovery sensitivity potential for $\tilde{\chi}_1^\pm\tilde{\chi}_2^0$ production and the exclusion sensitivity by about 300 GeV, assuming $\tilde{\chi}_1^\pm \to W\tilde{\chi}_1^0$ and $\tilde{\chi}_2^0 \to h\tilde{\chi}_1^0$. Future improvements

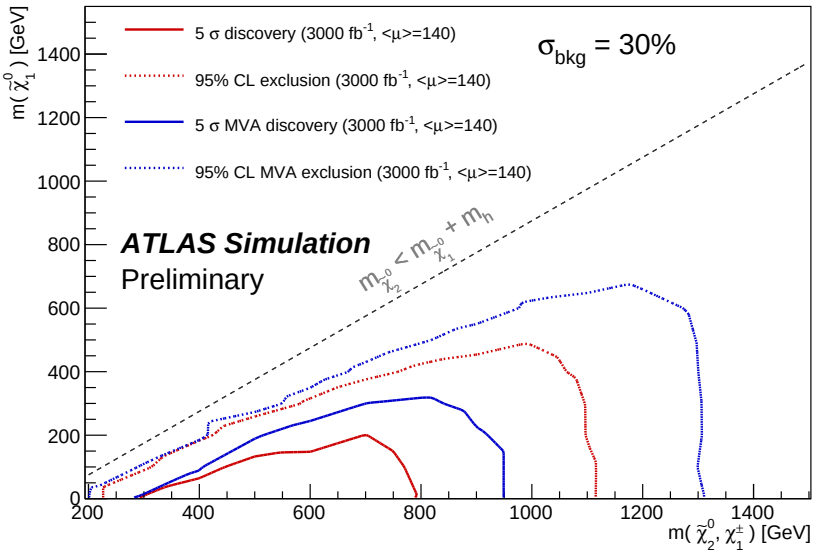

Figure 9: Expected 95% exclusion and discovery contours for the 3000 fb^{-1} luminosity scenario in the $m(\tilde{\chi}_1^0)$ vs $m(\tilde{\chi}_1^\pm,\tilde{\chi}_2^0)$ plane for the Wh-mediated simplified model, comparing the cut and count and MVA approaches.

in the understanding of experimental and theoretical systematic uncertainties on the SM background would provide additional potential for sensitivity gains at high luminosity on SUSY scenarios reported here and beyond.

References

[1] H. Miyazawa, Prog. Theor. Phys. **36** (1966) 1266.

[2] P. Ramond, Phys. Rev. **D 3** (1971) 2415.

[3] Y. Golfand, E. Likhtman, JETP Lett. **13** (1971) 323.

[4] A. Neveu, J. H. Schwarz, Nucl. Phys. **B 31** (1971) 86.

[5] A. Neveu, J. H. Schwarz, Phys. Rev. **D 4** (1971) 1109.

[6] J. L. Gervais, B. Sakita, Nucl. Phys. **B 34** (1971) 632.

[7] D. Volkov, V. Akulov, Phys. Lett. **B 46** (1973) 109.

[8] J. Wess, B. Zumino, Phys. Lett. **B 49** (1974) 52.

[9] J. Wess, B. Zumino, Nucl. Phys. **B 70** (1974) 39.

[10] ATLAS Collaboration, Phys.Lett. **B716** (2012) 1–29, arXiv:1207.7214.

[11] CMS Collaboration, Phys. Lett. B (2012) 30, arXiv:1207.7235.

[12] ATLAS Collaboration, JINST **3** (2008) S08003.

[13] ATLAS, CERN-LHCC-2012-022. LHCC-I-023 (2012). https://cds.cern.ch/record/1502664.

[14] https://twiki.cern.ch/twiki/bin/view/AtlasPublic/SupersymmetryPublicResults.

[15] ATLAS Collaboration, ATL-PHYS-PUB-2013-002.

[16] ATLAS Collaboration, ATL-PHYS-PUB-2014-010.

[17] ATLAS Collaboration, ATL-PHYS-PUB-2013-009.

[18] ATLAS Collaboration, ATL-PHYS-PUB-2013-004.

[19] T. Gleisberg *et al.*, JHEP **0902** (2009) 007, arXiv:0811.4622.

[20] T. Sjöstrand *et al.*, Comp. Phys. Comm. **135** (2001) 238, arXiv:hep-ph/0010017.

[21] J. M. Campbell and R. K. Ellis, Nucl. Phys. Proc. Suppl. **205-206** (2010) 10–15, arXiv:1007.3492 [hep-ph].

[22] J. Alwall *et al.*, JHEP **06** (2011) 128. 1106.0522.

[23] B. P. Kersevan and E. Richter-Was, Comput. Phys. Commun. **149** (2003) 142–194, arXiv:hep-ph/0201302 [hep-ph].

[24] P. Nason, JHEP **0411** (2004) 040, arXiv:hep-ph/0409146.

[25] M. Aliev *et al.*, Comput. Phys. Commun. **182** (2011) 1034, arXiv:1007.1327.

[26] J. Pumplin *et al.*, JHEP **0207** (012) 2002, arXiv:0802.0007.

[27] H. Lai *et al.*, Phys. Rev. **D 82** (2010) 074024, arXiv:1007.2241.

[28] M. Bahr et al., Eur. Phys. J. **C58** (2008) 639–707, arXiv:0803.0883 [hep-ph].

[29] T. Plehn, http://www.thphys.uni-heidelberg.de/˜ plehn/index.php?show=prospino.

[30] R. Barbieri and G. F. Giudice, Nucl.Phys. **B306** (1988) 63.

[31] B. de Carlos and J. A. Casas, Phys. Lett. **B309** (1993) 320–328, arXiv:hep-ph/9303291.

[32] ATLAS Collaboration, Eur.Phys.J. **C75** no. 5, (2015) 208, arXiv:1501.07110 [hep-ex].

[33] D. Tovey, JHEP **04** (2008) 034, arXiv:0802.2879 [hep-ph].

[34] J. T. Linnemann, arXiv:physics:0312059.